Thin-Walled Structures 141 (2019) 208–216

Contents lists available at ScienceDirect

Thin-Walled Structures

journal homepage: www.elsevier.com/locate/tws

Review

Stability and design of stainless steel structures – Review and outlook

Leroy Gardner

Imperial College London, UK

ARTICLE INFO

Keywords:
Buckling
Instability
Stainless steel
Strain hardening
Structural engineering

ABSTRACT

This paper provides a review of recent developments in research and design practice surrounding the structural use of stainless steel, with an emphasis on structural stability. The nonlinear stress-strain characteristics of stainless steel, which are discussed first, give rise to a structural response that differs somewhat from that of structural carbon steel. Depending on the type and proportions of the structural element or system, the nonlinear material response can lead to either a reduced or enhanced capacity relative to an equivalent component featuring an elastic, perfectly plastic material response. In general, in strength governed scenarios, such as the in-plane bending of stocky beams, the substantial strain hardening of stainless steel gives rise to capacity benefits, while in stability governed scenarios, the early onset of stiffness degradation results in reduced capacity. This behaviour is observed at all levels of structural response including at cross-sectional level, member level and frame level, as described in the paper. Current and emerging design approaches that capture this response are also reviewed and evaluated. Lastly, with a view to the future, the application of advanced analysis to the design of stainless steel structures and the use of 3D printing for the construction of stainless steel structures are explored.

1. Introduction

Stainless steel is a high-performance construction material that combines the strength and stiffness associated with ferrous alloys with the corrosion resistance derived principally from the high chromium content. This combination of properties comes at the cost, which puts increased emphasis on ensuring that the material is utilized to the utmost in structural applications. This requires developing a comprehensive understanding of the structural response and embracing advanced design and construction methods that may deviate from traditional and familiar practice.

Applications of stainless steel in construction date back about 90 years and include landmark examples such as the cladding on the Chrysler Building in New York and the Gateway Arch in St. Louis. More contemporary and somewhat less prominent examples, which emphasize the recent increased use of stainless steel for its desirable durability and structural properties rather than simply its aesthetics, include buildings, towers, domes, footbridges and road bridges, a selection of which is shown in Figs. 1–6: the Sanomatalo Building in Helsinki, in which stainless steel was used to form an exterior bracing system (Fig. 1) featuring cold-formed and welded structural sections and a range of connection details (Fig. 2), the Regent's Place Pavilion in London (Fig. 3), the Millennium footbridge in York featuring an 80 m span duplex stainless steel arch (Fig. 4), a footbridge (Fig. 5) near Siena, which used welded lean duplex stainless steel sections, and a road bridge (Fig. 6), also near Siena, which employed a duplex stainless steel circular hollow section arch as the main load-carrying element. Further information on the use of stainless steel in structural and offshore applications may be found in Refs. [1–4].

In this paper, the material stress-strain response of stainless steel is first discussed as this is fundamental to developing an understanding of the structural response at the cross-section, member and frame levels. Constitutive models to reflect the rounded stress-strain response of the material are reviewed and an overview is given to the importance of cold-working on enhancing the material strength of cold-formed stainless steel sections. The inelastic buckling and strain hardening response of stainless steel structural elements is then discussed in Section 3, together with an overview of design approaches that have been developed to reflect the influence of material nonlinearity and indeed take benefit from the pronounced strain hardening. In Section 4, with a view to the future, opportunities for the application of advanced design and construction methods to stainless steel structures are explored. Finally conclusions are drawn in Section 5.

2. Stress-strain response

There is a wide variety of stainless steel alloys, but all are characterized by a rounded stress–strain response with no sharply defined

E-mail address: Leroy.gardner@imperial.ac.uk.

https://doi.org/10.1016/j.tws.2019.04.019
Received 28 December 2018; Received in revised form 17 March 2019; Accepted 14 April 2019

Fig. 1. Sanomatalo building, Helsinki.

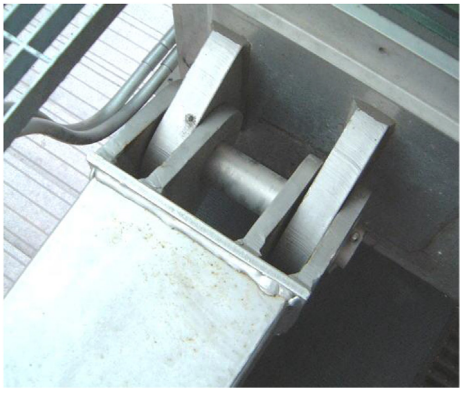

Fig. 2. Connection detail in the Sanomatalo Building, Helsinki.

Fig. 3. Regent's Place pavilion, London.

Fig. 4. Millennium bridge, York.

Fig. 5. Footbridge near Siena.

Fig. 6. Road bridge near Siena.

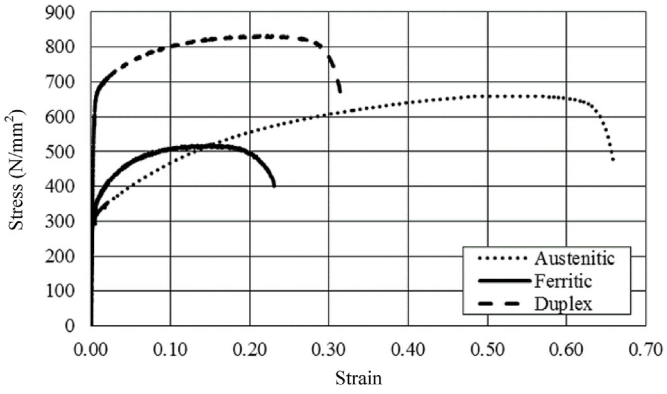

Fig. 7. Typical full stress-strain curves for three main families of stainless steel.

yield point, typically examples of which are shown in Figs. 7 and 8 for the three main families of stainless steel – austenitic, ferritic and duplex. Fig. 7 shows the full range stress-strain response, emphasizing the high ultimate-to-yield strength ratio and high ductility of stainless steel, particularly the austenitic grades, while Fig. 8 shows curves up to 1% strain and highlights the rounded stress-strain behaviour. This constitutive behaviour can be represented analytically by different material models, but the most common are based on the Ramberg–Osgood

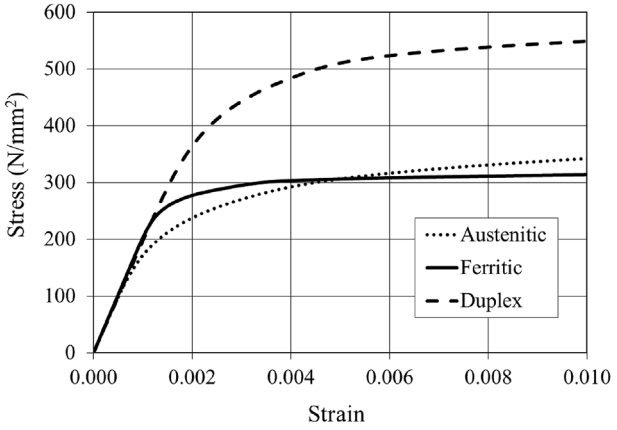

Fig. 8. Typical stress-strain curves for three main families of stainless steel up to 1% strain.

formulations or extensions thereof, which are reviewed below. The degree of roundedness, the level of strain hardening, the strain at ultimate stress and the ductility at fracture of the material all vary between grades, and need to be suitably captured for an accurate representation of the material to be achieved. The stress-strain properties, particularly the yield stress (or 0.2% proof stress) and ductility, are also influenced by the prior level of cold-work; structural stainless steel cross-sections are typically cold-formed, and cold-work may arise during forming of the flat sheet or during section forming.

The Ramberg-Osgood formulation was originally proposed to represent the rounded stress-strain (σ-ε) characteristics of aluminium [5] and is given in its most common form (as modified by Hill [6]) by Equation (1):

$$\varepsilon = \frac{\sigma}{E} + 0.002\left(\frac{\sigma}{f_y}\right)^n \tag{1}$$

where E is the Young's modulus, f_y is the 0.2% proof stress and n is a strain hardening exponent that defines the degree of roundedness of the curve. Equation (1) has been shown to be capable of accurately representing different regions of the stress–strain curve of stainless steel, depending on the choice of the n parameter, but found to be generally incapable of accurately representing the full stress–strain curve with a single value of n. This observation led to the development of a number of two-stage [7–9] (as well as three-stage [10] and multi-stage [11]) Ramberg–Osgood models that were capable of providing a single continuous representation of the stress–strain curve of stainless steel from the onset of loading to the ultimate tensile stress. The two-stage model proposed by Mirambell and Real [7] utilizes Equation (1) up to the 0.2% proof stress, and Equation (2) thereafter, up to the ultimate tensile stress:

$$\varepsilon = \frac{\sigma - f_y}{E_{0.2}} + \left(\varepsilon_u - \varepsilon_{0.2} - \frac{f_u - f_y}{E_{0.2}}\right)\left(\frac{\sigma - f_y}{f_u - f_y}\right)^m + \varepsilon_{0.2} \quad \text{for } \sigma > f_y \tag{2}$$

where $E_{0.2}$ is the tangent modulus at the 0.2% proof stress, f_u is the ultimate tensile stress, ε_u is the ultimate strain, $\varepsilon_{0.2}$ is the total strain at the 0.2% proof stress and m is the second strain hardening exponent. Rasmussen [8] presented a simplified version of Equation (2), noting that for ductile materials:

$$\varepsilon_u \approx \varepsilon_u - \varepsilon_{0.2} - \frac{f_u - f_y}{E_{0.2}} \tag{3}$$

leading to Equation (4):

$$\varepsilon = \frac{\sigma - f_y}{E_{0.2}} + \varepsilon_u\left(\frac{\sigma - f_y}{f_u - f_y}\right)^m + \varepsilon_{0.2} \quad \text{for } \sigma > f_y \tag{4}$$

Crucial to the use of the two-stage Ramberg-Osgood model are the five input parameters – the Young's modulus E and 0.2% proof stress f_y, values of which are readily available in material standards and will typically be known to the user, as well as the strain at the ultimate tensile stress ε_u and the strain hardening exponents n and m, which are not specified in material standards. Means of predicting these latter three parameters are therefore important and have been the subject of much recent research. In Annex C of EN 1993-1-4 [12], the predictive models of Rasmussen [8] have been employed, while recent extensions to these models have been made by Arrayago et al. [13], as well as by Gardner and Yun [14] for application to cold-formed steel, which are included in the Fourth Edition of the European Design Manual for Structural Stainless Steel [15] and are expected to be included in future revisions of Eurocode 3 Part 1.4.

The two-stage Ramberg-Osgood expression has also been applied to the modelling of stainless steel material behaviour at elevated temperature [16], where the second strain hardening exponent m (denoted m_θ at elevated temperature) can be defined explicitly with reference to the strength at 2% strain $f_{2,\theta}$, which is value provided in structural fire design standards including EN 1993-1-2 [17]. The elevated temperature stress-strain is forced to pass through $f_{2,\theta}$ at 2% strain by defining m_θ as given in Equation (5) [18], where $f_{p0.2,\theta}$ is the elevated temperature 0.2% proof stress and other symbols are as previously defined with θ denoting elevated temperature. Note that the first strain hardening parameter n_θ is defined in the same manner as at room temperature.

$$m_\theta = \frac{\ln\left(\frac{\varepsilon_{u,\theta}}{0.02 - \varepsilon_{0.2,\theta} - \frac{f_{2,\theta} - f_{p0.2,\theta}}{E_{0.2,\theta}}}\right)}{\ln\left(\frac{f_{u,\theta} - f_{p0.2,\theta}}{f_{2,\theta} - f_{p0.2,\theta}}\right)} \tag{5}$$

To date, the above analytical expressions have been used primarily by researchers in finite element simulations, though do also feature in part in some current structural design formulae, as described in Section 3. However, with the increasing use of design by advanced analysis, such expressions are becoming ever more important for practical application, and for this reason are expected to feature in a new European Standard for design by finite element analysis, which is currently in development.

In addition to the rounded stress-strain response of stainless steel, another key feature of the material properties of cold-formed stainless steel cross-sections is the pronounced influence of cold-work. Essentially, plastic deformation experienced during the cold-forming of stainless steel cross-sections results in an increase in strength and a loss in ductility. While this effect is also present in conventional cold-formed carbon steel sections, it is more significant in stainless steel sections due to the shape of the stress-strain curve and the high ratio of ultimate to yield strength.

A number of studies [19–23] have been carried out to predict and harness the influence of cold-work on the material properties of stainless steel cross-sections. The predictive expressions of Rossi et al. [21] are included in the Fourth Edition of the European Design Manual for Structural Stainless Steel [15] and are expected to be included in future revisions of Eurocode 3 Part 1.4. In the developed predictive expressions, the enhanced yield strength is presented as a function of the basic properties of the unformed material (i.e. the yield strength and ultimate tensile strength) and the approximate level of strain induced during forming, expressed in terms of the geometry of the formed section.

3. Accounting for material nonlinearity in structural design

The nonlinear material stress-strain response described in Section 2 has a direct influence on the structural behaviour of stainless steel cross-sections, members and frames, as well as connections [24–29]. The observed behaviour, together with existing and emerging design

treatments, are described in this section.

3.1. Material nonlinearity at cross-section level

Structural cross-sections have a variety of geometric proportions. Those containing slender elements are referred to as Class 4 or slender cross-sections and are characterized by failure due to local buckling occurring prior to the attainment of the yield resistance, while those of stockier proportions (termed Class 1–3) fail beyond this point and benefit from the spread of plasticity and strain hardening. The implications of the rounded stress-strain curve of stainless steel are that Class 4 cross-sections experience inelastic local buckling below the 0.2% proof stress while Class 1–3 cross-sections undergo inelastic local buckling beyond the 0.2% proof stress and can benefit from the substantial strain hardening exhibited by the material. For the former, modified effective width expressions [30] are included in Eurocode 3: Part 1.4, while for the latter, modified slenderness limits (i.e. limiting width-to-thickness ratios) [30] are adopted in Eurocode 3: Part 1.4 and the continuous strength method has been developed. Modified strength curves in the Direct Strength Method (DSM) framework have also been proposed. For cross-sections under combined axial compression and bending, the same interaction formulae are adopted for stainless steel in Eurocode 3: Part 1.1.

The continuous strength method is a deformation based design approach that departs from the traditional practice of placing cross-sections into behavioural classes, and instead presents resistance as a continuous function of the slenderness of the cross-section. The maximum strain that a cross-section can endure ε_{csm} prior to failure by local buckling is determined from the 'base curve', while strain hardening is allowed for through the adoption of a material model that includes strain hardening. The base curve, derived on the basis of a regression fit to existing compression and bending test data for a range of metallic materials, including austenitic, duplex and ferritic stainless steels, carbon steel, high strength steel and aluminium, defines the relationship between the deformation capacity, expressed in terms of the strain ratio ($\varepsilon_{csm}/\varepsilon_y$) and the local slenderness $\bar{\lambda}_p$ of the full cross-section. This relationship is given by Equation (6) [31] and Equation (7) [32] for non-slender ($\bar{\lambda}_p \leq 0.68$) and slender ($\bar{\lambda}_p > 0.68$) plated sections, respectively, where $\varepsilon_y = f_y/E$ is the yield strain and $\bar{\lambda}_p$ is the cross-section slenderness, calculated as $\sqrt{f_y/\sigma_{cr}}$, in which σ_{cr} is the elastic local buckling stress of the full cross-section under the applied loading conditions, which may be determined using simplified analytical expressions [33,34] or numerical tools such as the finite strip software CUFSM [35]. Two limits are applied to the strain ratio ($\varepsilon_{csm}/\varepsilon_y$) given by Equation (6) for non-slender cross-sections: the first limit Ω is a project dependent design parameter that defines the permissible level of plastic deformation, with a recommended value of 15, while the second limit, which is related to the adopted elastic, linear hardening material model, is to avoid over-prediction of the material strength. The base curves for non-slender and slender cross-sections meet at the slenderness limit ($\bar{\lambda}_p = 0.68$), where the strain ratio $\varepsilon_{csm}/\varepsilon_y$ is equal to unity.

$$\frac{\varepsilon_{csm}}{\varepsilon_y} = \frac{0.25}{\bar{\lambda}_p^{3.6}} \text{but} \leq \min\left(\Omega, \frac{C_1\varepsilon_u}{\varepsilon_y}\right) \text{ for } \bar{\lambda}_p \leq 0.68 \tag{6}$$

$$\frac{\varepsilon_{csm}}{\varepsilon_y} = \left(1 - \frac{0.222}{\bar{\lambda}_p^{1.050}}\right)\frac{1}{\bar{\lambda}_p^{1.050}} \text{for } \bar{\lambda}_p > 0.68 \tag{7}$$

The CSM elastic, linear hardening material model, which features four material coefficients (C_1, C_2, C_3 and C_4), is illustrated in Fig. 9, with the strain hardening slope E_{sh} calculated from Equation (8). Values of the coefficients for each stainless steel grade were calibrated based on the material tensile coupon test data by means of least squares regression, and are summarised in Table 1 [36]. The CSM material model parameter C_1 is used to define a cut-off strain (see Equation (6)) to prevent over-predictions of strength from the linear hardening material model. The CSM material coefficient C_2 is employed in Equation (8) to define the strain hardening slope E_{sh}, while the parameter $\varepsilon_u = C_3(1–f_y/f_u) + C_4$ (though the coefficient C_4 is zero for stainless steels) is the predicted strain corresponding to the material ultimate strength f_u. The CSM material model accounts for strain hardening, and thus represents better the actual nonlinear material stress–strain characteristics of stainless steels, compared with the traditional elastic, perfectly-plastic material model adopted in the current European code EN 1993-1-4 [12].

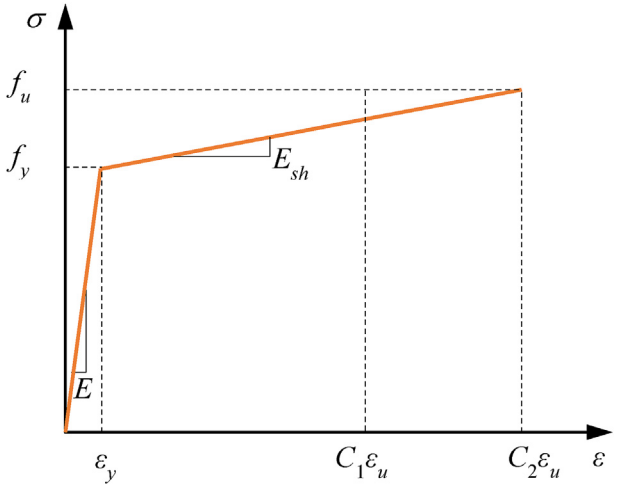

Fig. 9. CSM material stress-strain model.

Table 1
Coefficients for CSM material model.

Stainless steel grade	C_1	C_2	C_3
Austenitic	0.1	0.16	1.0
Duplex	0.1	0.16	1.0
Ferritic	0.4	0.45	0.6

$$E_{sh} = \frac{f_u - f_y}{C_2\varepsilon_u - \varepsilon_y} \tag{8}$$

Upon determination of the design local bucking limiting strain ε_{csm} and the corresponding strain hardening modulus E_{sh}, the CSM design stress σ_{csm} for cross-section in compression can be calculated from Equation (9) for non-slender sections with a design strain greater than or equal to the yield strain ($\varepsilon_{csm}/\varepsilon_y \geq 1$) and Equation (10) for slender sections with a design strain less than the yield strain ($\varepsilon_{csm}/\varepsilon_y < 1$). Note that Equation (9) represents the strain hardening behaviour of the material through the strain hardening modulus E_{sh}. The CSM cross-section compression resistance $N_{csm,Rd}$ is directly calculated as the product of the CSM design stress σ_{csm} and the cross-section area A, as given by Equation (11), where γ_{M0} is a partial factor for cross-section resistance, with a recommended value of 1.1 for stainless steel.

$$\sigma_{csm} = f_y + E_{sh}(\varepsilon_{csm} - \varepsilon_y) \text{for } \varepsilon_{csm}/\varepsilon_y \geq 1 \tag{9}$$

$$\sigma_{csm} = E\varepsilon_{csm} \text{for } \varepsilon_{csm}/\varepsilon_y < 1 \tag{10}$$

$$N_{csm,Rd} = \frac{A\sigma_{csm}}{\gamma_{M0}} \tag{11}$$

For cross-sections in bending about an axis of symmetry, the design maximum attainable outer-fibre strain ε_{csm} is determined from Equations (6) and (7) for non-slender and slender sections, respectively. The design stress distribution can then be derived based on the elastic, linear hardening material model. For slender sections with a design

strain ratio less than unity, there is an elastic, linear-varying stress distribution and no benefit arises from strain hardening; the bending moment resistance $M_{csm,Rd}$ is thus directly calculated as the elastic bending moment resistance multiplied by the strain ratio, as given by Equation (12), where W_{el} is the elastic section modulus. For non-slender sections with a design strain ratio greater than or equal to unity, $M_{csm,Rd}$ was firstly derived analytically through integration of the design stress distribution throughout the cross-section depth, and then transformed into simplified design formula, as given by Equation (13), where W_{pl} is the plastic section modulus and α is the CSM bending coefficient, related to cross-section shape and axis of bending: for tubular sections (e.g., CHS, SHS and RHS) bending about either axis and for I-sections under major axis bending, α is equal to 2.0, while for I-sections in minor axis bending, $\alpha = 1.2$ [31,36].

$$M_{csm,Rd} = \frac{\varepsilon_{csm}}{\varepsilon_y}\frac{W_{el}f_y}{\gamma_{M0}} \quad \text{for } \varepsilon_{csm}/\varepsilon_y < 1 \tag{12}$$

$$M_{csm,Rd} = \frac{W_{pl}f_y}{\gamma_{M0}}\left[1 + \frac{E_{sh}}{E}\frac{W_{el}}{W_{pl}}\left(\frac{\varepsilon_{csm}}{\varepsilon_y} - 1\right) - \left(1 - \frac{W_{el}}{W_{pl}}\right) \text{ for } \varepsilon_{csm}/\varepsilon_y \geq 1 \right. \\ \left. \Big/\left(\frac{\varepsilon_{csm}}{\varepsilon_y}\right)^{\alpha}\right] \tag{13}$$

For cross-sections under combined loading, use of the Eurocode interaction formulae, but anchored to the CSM end points for axial compression and bending has been shown to provide accurate resistance predictions. Application of the CSM resistance functions has been shown consistently [31,32,37–41] to yield improved capacity predictions over traditional methods and has now been incorporated into structural design guidance in North America [42] and Europe [15]. Inclusion is anticipated in the next revision of EN 1993-1-4.

Other forms of localized cross-section failure include shear buckling [43,44], distortional buckling [45] and failure (typically termed web crippling in the context of cold-formed sections) under concentrated transverse forces [46–49]. In each case, similar trends as seen for local buckling are also observed i.e. the rounded stress-strain response creates the need for modified buckling curves (and DSM strength curves) in the slender range [50–53] where failure occurs below the plastic resistance, while for stockier sections, strain hardening enables increased load-bearing capacities beyond the plastic resistance [47,49]. Tentative proposals have been made to extend the CSM to the design of cross-sections in shear [54], while extension to failure under concentrated transverse loads remains a topic for future research.

3.2. Material nonlinearity at member level

Inelastic buckling is the key concern for the design of stainless steel members. In EN 1993-1-4, the influence of the rounded stress-strain response is considered indirectly through adjustment to the plateau length (i.e. the slenderness below which there is no reduction to cross-section resistance) and imperfection factor of the Perry-Robertson based buckling curves. In the current version of the code, these parameters only vary with section type and axis of buckling, while in the recently published Fourth Edition of the European Design Manual for Structural Stainless Steel [15], there is also variation with material grade (austenitic, ferritic or duplex), reflecting the varying degree of material nonlinearity; these revised buckling curves are expected to be included in future revisions of Eurocode 3 Part 1.4. A similar approach is used in the Chinese Standard for structural stainless steel design CECS-410 [55].

In US design provisions for cold-formed stainless steel [56], the material nonlinearity is accounted for explicitly in column design through the use of the tangent stiffness approach. This utilizes the tangent modulus corresponding to the buckling stress in place of the Young's modulus in the traditional Euler buckling equation; the results are generally accurate, but the method is inherently iterative.

In the Australian/New Zealand Standard for stainless steel structures AS/NZS 4673 [57], a hybrid approach that features the basic form of the Perry-Robertson equation, but with additional terms to account for the material nonlinearity, is utilized. This approach was developed by Rasmussen and Rondal [58] and instead of requiring knowledge of the full stress-strain curve of the material, as required in the tangent modulus approach, only two parameters, namely the strain hardening coefficient from the Ramberg-Osgood model n and a nondimensional proof stress $e = f_y/E$, are used to reflect the degree of material nonlinearity. This enables the practicality of the Perry-Robertson formulation to be retained, but also allows the influence of the material nonlinearity to be explicitly captured, resulting in accurate predictions of column buckling strength.

Progress towards extension of the Direct Strength Method [59,60] and the Continuous Strength Method [61–63] to the design of stainless steel members has also been made. There now exists a significant body of member buckling test and numerical data on stainless steel compression members [64–70], beams [71] as well as beam-columns [72–77], particularly on tubular cross-sections, against which these new design methods can be evaluated. Although the influence of material nonlinearity on stainless steel beam design is considered in EN 1993-1-4 [12] in deflection calculations (through the use of the secant modulus) and in lateral torsional buckling calculations (though the definition of buckling curves), the stability design of stainless steel members in flexure has received significantly less attention than in compression. Ongoing research is currently addressing this shortcoming, and further work is anticipated in this area.

3.3. Material nonlinearity at frame level

Material nonlinearity also affects the behaviour of the stainless steel structures at the frame level, but no explicit guidance on the treatment of material nonlinearity in global analyses is currently given in EN 1993-1-4. In the absence of guidance, an elastic analysis may be assumed to be acceptable for stainless steel frames, though recent research [78] has shown that this is not necessarily the case. The gradual degradation of material stiffness was shown in some instances to significantly affect the characteristics of the structural system and the subsequent distribution of internal forces and moments. If material nonlinearity is considered in the global analysis of a frame, greater deformations result due to the loss of material stiffness; if plasticity is ignored, peak moments are typically underpredicted. It was therefore recommended [78] that plastic analysis (employing the rounded material stress-strain response described in Section 2) should always be conducted for determining the internal forces and moments in stainless steel frames.

Considering geometric nonlinearities at the frame level, EN 1993-1-1 [79] and other international steel design standards state that second order effects may be neglected provided α_{cr} is greater than or equal to 10 when an elastic analysis is employed, with α_{cr} being the factor by which the design loading on a frame has to be increased to cause overall buckling in a global sway mode. However, when plastic analysis is employed, yielding of the material degrades the stiffness of the structure, and hence a stricter requirement of $\alpha_{cr} \geq 15$ is prescribed in EN 1993-1-1 before second order effects can be neglected. Use of a single limit of 15 for any structural system is however considered to be overly simplistic, both for stainless steel and indeed carbon steel frames [80]. A more consistent and accurate approach is to determine the degree of stiffness degradation and hence the increased susceptibility to second order effects on a frame by frame basis, as proposed in Refs. [78,80], where a modified elastic buckling load factor $\alpha_{cr,mod}$, which considers explicitly the reduction in frame stiffness following plasticity at a given design load, is presented. The method is implemented by performing a first order plastic analysis of the structure and determining the secant stiffness K_s at the design load level, relative to the initial stiffness K, as illustrated in Fig. 10.

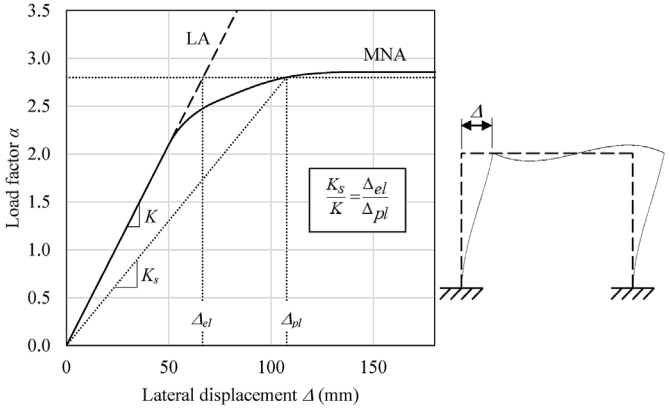

Fig. 10. Reduction to global sway stiffness as a result of material nonlinearity [78].

The modified elastic buckling load factor $\alpha_{cr,mod}$ is then calculated from Equation (14), utilizing the derived secant stiffness, and susceptibility to second order effects is assessed on the basis of the value of $\alpha_{cr,mod}$, relative to a common limit (for both plastic and elastic analysis) of 10. If $\alpha_{cr} \geq 10$, second order effects may be neglected. Note that the 0.8 factor approximates the further loss of stiffness due to the additional plastification that occurs at the same load level when second order effects are considered, as described in Refs. [78,80]. This approach provides a consistent treatment of second order effects for both elastic and plastic analysis.

$$\alpha_{cr,mod} = 0.8\frac{K_s}{K}\alpha_{cr} \tag{14}$$

The applicability and accuracy of the proposed method has been demonstrated through comparisons with numerical results on a series of stainless steel frames [78]. Comparisons with results from parallel work on carbon steel frames has also yielded similar findings [80]. Further work is currently underway on this topic.

4. Outlook

The future of structural engineering is exciting; among other developments, integrated advanced analysis and design is already beginning to play an important role in practice and 3D printing, though some way off mainstream applications, is offering revolutionary potential to the industry. The use of high performance materials such as stainless steel, with its excellent durability characteristics, is also likely to become more widespread in the future to respond to ever growing demands on the resilience and longevity of structures. With an emphasis on these topics, an outlook for the use of stainless steel in structural applications in the years to come is presented in this section.

4.1. Design by advanced analysis

In conventional design, a first order elastic analysis is typically performed and the structural system is treated as a set of individual beams, columns and connections. System effects are approximated through effective length factors, inelastic load redistribution beyond first yield is not captured, and time-consuming, semi-empirical design calculations are required for each individual member of the frame. This typically leads to inefficiencies in design-time, unnecessary reliance on engineering approximations, excessive use of construction materials, and can result in unsafe design. For all construction materials, but particularly for high value structural materials where efficient design is paramount to promote and justify more widespread usage, the opportunities offered by more advanced techniques should be further explored and exploited.

An alternative approach to that described above is to carry out a system-level advanced analysis, typically incorporating both geometric and material nonlinearities, as well as imperfections [81–89]. In such an approach, the interactions between the individual structural components are directly captured, the distribution of forces and moments in the frame is accurately reflected, including allowance for redistribution, and the required design checks are greater reduced, since the key structural phenomena (principally yielding and buckling) are triggered and free to occur within the analysis. Only cross-section capacity checks will typically be required when the structure is simulated using beam elements, and a geometrically and materially nonlinear analysis with imperfections (GMNIA) is employed. An alternative to carrying out cross-section checks is to limit the maximum strain that arises in the structure based on the local slenderness of the adopted cross-sections [34,90]; the maximum strain can be determined from the CSM base curve [31,32].

Design by advanced analysis can be used to verify the design of the members within structural frames, though, at present, connection design would generally have to be treated separately [81]. However, with greater use of 3D CAD and building information modelling (BIM), it is envisaged that these more detailed aspects could also be brought under the umbrella of design by advanced analysis in the future. The opportunities offered by design by advanced analysis for a more streamlined, integrated, system-level design approach are clear, as are the implications on the education and training of engineers [81]. The approach is particularly suitable for application to stainless steel structures due to the high material value and the complexities presented by the rounded material stress-strain response for traditional design treatments.

4.2. Stainless steel 3D printing

Stainless steel is a high value material which lends itself to the emerging opportunities associated with metal 3D printing. The ability to place material in the optimal configuration to resist the applied load, rather than being limited by the constraints of traditional fabrication processes, brings clear opportunities. Such opportunities exist both in terms of improved sustainability, associated with a reduction in material consumption, and improved economy, associated with lower material costs. Although 3D printing can be applied to a range of metals, cost savings are particularly important for materials with a high initial cost such as stainless steel. Early research into the behaviour of metal 3D printed structural elements has been reported in Ref. [91], while a review of the methods, research, applications, opportunities and challenges for this technology has been presented in Ref. [92].

It has been identified [92] that the two principal methods of metal 3D printing that are currently suited to construction-scale applications are powder-bed fusion (PBF) and directed energy deposition (DED). Deformed stainless steel test samples printed using powder bed fusion are shown in Fig. 11. The test specimens were built to a high degree of geometric accuracy, while the rapid cooling associated with the as-built specimens resulted in high material strengths. The Young's modulus

Fig. 11. Tested powder bed fusion 3D printed stainless steel stub columns [91].

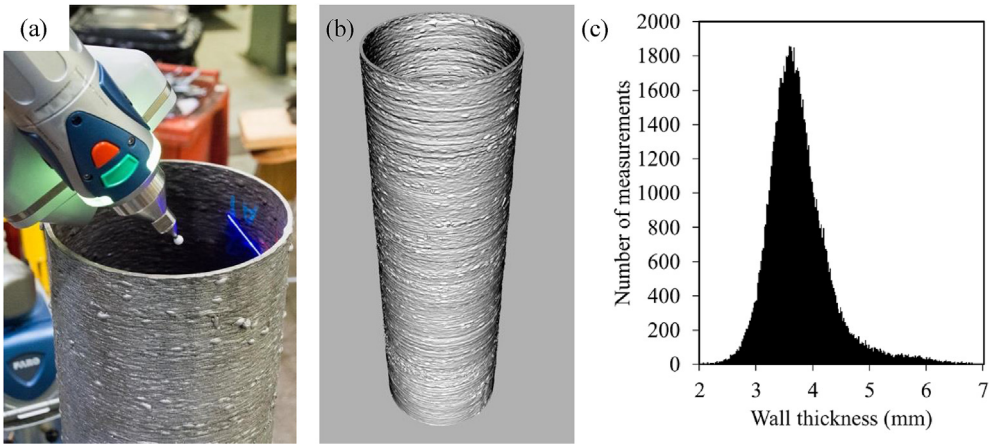

Fig. 12. (a) 3D laser scanning of a WAAM stainless steel circular hollow section, (b) the digital representation of the scanned specimen and (c) the measured variation in the wall thickness.

was however slightly lower (by around 10%) than equivalent material produced using traditional methods. Following preliminary comparisons, existing structural design provisions [12,15] were shown to be generally applicable to cross-sections built in this manner.

Research into material produced using directed energy deposition, specifically wire arc additive manufacturing (WAAM), has also been carried out at Imperial College London [92,93] in support of the verification of the 10.5 m span MX3D bridge, which was 3D printed from Grade 308LSi austenitic stainless steel [92]. Advanced 3D laser scanning has been employed in the research to measure the specimen geometry enabling the undulating surface topography, that results in varying wall thicknesses, to be captured. Scanning of a typical stainless steel test specimen is shown in Fig. 12(a), the digital representation of the scanned specimen is shown in Fig. 12(b) and the wall thickness distribution is reproduced in Fig. 12(c), the latter clearly indicating greater variation than seen with conventionally manufactured sections. Full scale load testing of the bridge has also been performed, as shown in Fig. 13 for horizontal loading of the handrails and Fig. 14 for vertical loading. The complete 3D printed stainless steel bridge is shown in Fig. 15.

Additive manufacturing offers many opportunities for the construction sector, but there will also be fresh challenges and demands. A new way of thinking will be required for the design and verification of structures, and there will be greater emphasis on the use of advanced analysis, as well as inspection and load testing.

Fig. 13. Horizontal load testing of handrails of MX3D bridge.

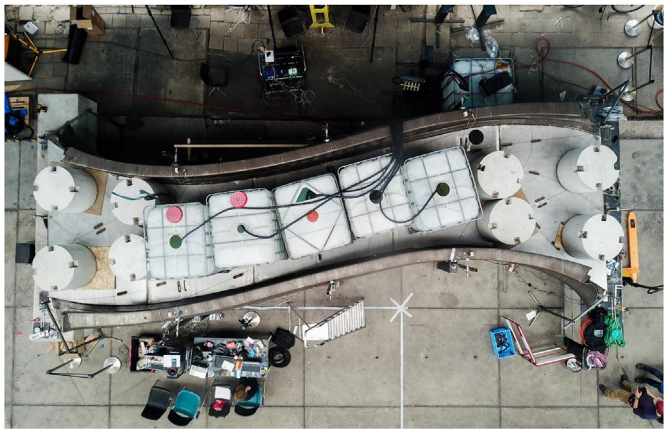

Fig. 14. Vertical load testing of MX3D bridge.

Fig. 15. MX3D bridge at Dutch Design Week, 2018.

5. Conclusions

Stainless steel is a high performance structural material, with properties that make it well suited to a range of demanding engineering applications. Its chemical composition results in a characteristic rounded stress-strain curve that differs markedly for the sharply defined yielding behaviour typically observed for structural carbon steel. A series of constitutive models have been developed to represent this

behaviour, as summarised herein. The nonlinear material stress-strain response has a direct influence on the structural behaviour of stainless steel cross-sections, members and frames. At the cross-section level, capturing the inelastic local buckling in slender sections, as well as the substantial strain hardening in more stocky sections are the key design challenges; this requires deviation from the traditional elastic, perfectly plastic representation of the material stress-strain response used in traditional design and has led to the development of the deformation based continuous strength method of design. At the member and frame levels, appropriate allowance for the premature loss of stiffness is also required, and the latest and more promising design treatments and developments have been highlighted herein. With stainless steel being a high value material, its efficient use is paramount, and this is a particular incentive to embrace the latest analysis, design and construction technologies in the future.

References

[1] N.R. Baddoo, Stainless steel in construction: a review of research, applications, challenges and opportunities, J. Constr. Steel Res. 64 (11) (2008) 1199–1206.
[2] L. Gardner, The use of stainless steel in structures, Prog. Struct. Eng. Mater. 7 (2) (2005) 45–55.
[3] L. Gardner, Aesthetics, economics and design of stainless steel structures, Adv. Steel Constr. 4 (2) (2008) 113–122.
[4] F. Wang, L.H. Han, Analytical behavior of carbon steel-concrete-stainless steel double-skin tube (DST) used in submarine pipeline structure", Mar. Struct. 63 (2019) 99–116.
[5] W. Ramberg, W.R. Osgood, "Description of Stress–Strain Curves by Three Parameters", Technical Note No. 902, National Advisory Committee for Aeronautics, Washington, D.C., USA, 1943.
[6] H.N. Hill, "Determination of Stress–Strain Relations from Offset Yield Strength Values", Technical Note No. 927, National Advisory Committee for Aeronautics, Washington, D.C., USA, 1944.
[7] E. Mirambell, E. Real, On the calculation of deflections in structural stainless steel beams: an experimental and numerical investigation, J. Constr. Steel Res. 54 (4) (2000) 109–133.
[8] K.J.R. Rasmussen, Full-range stress–strain curves for stainless steel alloys", J. Constr. Steel Res. 59 (1) (2003) 47–61.
[9] L. Gardner, M. Ashraf, Structural design for non-linear metallic materials, Eng. Struct. 28 (6) (2006) 926–934.
[10] W.M. Quach, J.G. Teng, K.F. Chung, "Three-stage full-range stress–strain model for stainless steels", J. Struct. Eng., ASCE 134 (9) (2008) 1518–1527.
[11] P. Hradil, A. Talja, E. Real, A. Mirambell, B. Rossi, Generalized multistage mechanical model for nonlinear metallic materials, Thin-Walled Struct. 63 (2013) 63–69.
[12] EN 1993-1-4:2006 + A1:2015, Eurocode 3: Design of Steel Structures - Part 1–4: General Rules - Supplementary Rules for Stainless Steels, European Committee for Standardization (CEN), Brussels, 2015.
[13] I. Arrayago, E. Real, L. Gardner, Description of stress-strain curves for stainless steel alloys, Mater. Des. 87 (2015) 540–552.
[14] L. Gardner, X. Yun, Description of stress-strain curves for cold-formed steels, Constr. Build. Mater. 189 (2018) 527–538.
[15] SCI, Design Manual for Structural Stainless Steel", fourth ed., SCI Publication No. P413. *The Steel Construction Institute*, UK, 2017.
[16] L. Gardner, A. Insausti, K.T. Ng, M. Ashraf, Elevated temperature material properties of stainless steel alloys, J. Constr. Steel Res. 66 (5) (2010) 634–647.
[17] EN 1993-1-2, Eurocode 3, Design of Steel Structures - Part 1–2: General Rules – Structural Fire Design, European Committee for Standardization (CEN), Brussels, 2005.
[18] Y. Liang, T. Manninen, O. Zhao, F. Walport, L. Gardner, Elevated temperature material properties of a new high-chromium austenitic stainless steel, J. Constr. Steel Res. 152 (2019) 261–273.
[19] R.B. Cruise, L. Gardner, Strength enhancements induced during cold forming of stain-less steel sections, J. Constr. Steel Res. 64 (11) (2008) 1310–1316.
[20] S. Afshan, B. Rossi, L. Gardner, "Strength enhancements in cold-formed structural sections – Part I: material testing", J. Constr. Steel Res. 83 (2013) 177–188.
[21] B. Rossi, S. Afshan, L. Gardner, "Strength enhancements in cold-formed structural sections – Part II: predictive models", J. Constr. Steel Res. 83 (2013) 189–196.
[22] W.M. Quach, P. Qiu, Strength and ductility of corner materials in cold-formed stainless steel sections, Thin-Walled Struct. 83 (2014) 28–42.
[23] J. Wang, G. Shu, B. Zheng, Q. Jiang, Investigations on cold-forming effect of cold-drawn duplex stainless steel tubular sections, J. Constr. Steel Res. 152 (2019) 81–93.
[24] E.L. Salih, L. Gardner, D.A. Nethercot, Numerical investigation of net section failure in stainless steel bolted connections, J. Constr. Steel Res. 66 (12) (2010) 1455–1466.
[25] E.L. Salih, L. Gardner, D.A. Nethercot, Numerical study of stainless steel gusset plate connections, Eng. Struct. 49 (2013) 448–464.
[26] M. Elflah, M. Theofanous, S. Dirar, H. Yuan, "Behaviour of stainless steel beam-to-column joints — Part 1: experimental investigation", J. Constr. Steel Res. 152 (2019) 183–193.
[27] Y. Cai, B. Young, Structural behaviour of cold-formed stainless steel bolted connections at post-fire condition, J. Constr. Steel Res. 152 (2019) 213–321.
[28] Y. Cai, B. Young, Bearing resistance design of stainless steel bolted connections at ambient and elevated temperatures, Steel Compos. Struct. 29 (2) (2018) 273–286.
[29] Y. Cai, B. Young, High temperature tests of cold-formed stainless steel double shear bolted connections, J. Constr. Steel Res. 104 (2015) 49–63.
[30] L. Gardner, M. Theofanous, Discrete and continuous treatment of local buckling in stainless steel elements, J. Constr. Steel Res. 64 (11) (2008) 1207–1216.
[31] S. Afshan, L. Gardner, The continuous strength method for structural stainless steel design, Thin-Walled Struct. 68 (4) (2013) 42–49.
[32] O. Zhao, S. Afshan, L. Gardner, Structural response and continuous strength method design of slender stainless steel cross-sections, Eng. Struct. 140 (2017) 14–25.
[33] M. Seif, B.W. Schafer, Local buckling of structural steel shapes, J. Constr. Steel Res. 66 (10) (2010) 1232–1247.
[34] L. Gardner, A. Fieber, L. Macorini, Formulae for calculating elastic local buckling stresses of full structural cross-sections, Structures 17 (2019) 2–20.
[35] B.W. Schafer, S. Ádány, Buckling analysis of cold-formed steel members using CUFSM: conventional and constrained finite strip methods, Proceedings of the Eighteenth International Speciality Conference on Cold-Formed Steel Structures, Orlando, USA, 2006.
[36] C. Buchanan, L. Gardner, A. Liew, The continuous strength method for the design of circular hollow sections, J. Constr. Steel Res. 118 (2016) 207–216.
[37] H.X. Yuan, Y.Q. Wang, Y.J. Shi, L. Gardner, Stub column tests on stainless steel built-up sections, Thin-Walled Struct. 83 (2014) 103–114.
[38] K. Sachidananda, K.D. Singh, Numerical study of fixed ended lean duplex stainless steel (LDSS) flat oval hollow stub column under pure axial compression, *Thin-Walled* Struct. 96 (2015) 105–119.
[39] O. Zhao, L. Gardner, B. Young, Behaviour and design of stainless steel SHS and RHS beam-columns, Thin-Walled Struct. 106 (2016) 330–345.
[40] B. Zheng, G. Shu, L. Xin, R. Yang, Q. Jiang, Study on the bending capacity of cold-formed stainless steel hollow sections, Structures 8 (2016) 63–74.
[41] Y. Sun, O. Zhao, Material response and local stability of high-chromium stainless steel welded I-sections, Eng. Struct. 178 (2019) 212–226.
[42] AISC, "AISC Design Guide 27: Structural Stainless Steel", (2013) Chicago, USA.
[43] E. Real, E. Mirambell, I. Estrada, Shear response of stainless steel plate girders, Eng. Struct. 29 (7) (2007) 1626–1640.
[44] N. Saliba, L. Gardner, Experimental study of the shear response of lean duplex stainless steel plate girders, Eng. Struct. 46 (2013) 375–391.
[45] M. Lecce, K.J.R. Rasmussen, Distortional buckling of cold-formed stainless steel sections: experimental investigation, J. Struct. Eng., ASCE 132 (4) (2006) 497–504.
[46] H.T. Li, B. Young, Web crippling of cold-formed ferritic stainless steel square and rectangular hollow sections, Eng. Struct. 176 (2018) 968–980.
[47] G.B. dos Santos, L. Gardner, M. Kucukler, Experimental and numerical study of stainless steel I-sections under concentrated internal one-flange and internal two-flange loading, Eng. Struct. 175 (2018) 355–370.
[48] Y. Cai, B. Young, Web crippling of lean duplex stainless steel tubular sections under concentrated end bearing loads, Thin-Walled Struct. 134 (2019) 29–39.
[49] G.B. dos Santos, L. Gardner, Testing and numerical analysis of stainless steel I-sections under concentrated end-one-flange loading, J. Constr. Steel Res. 157 (2019) 271–281.
[50] M. Bock, E. Real, Strength curves for web crippling design of cold-formed stainless steel hat sections, Thin-Walled Struct. 85 (2014) 93–105.
[51] N. Saliba, E. Real, L. Gardner, Shear design recommendations for stainless steel plate girders, Eng. Struct. 59 (2014) 220–228.
[52] M. Lecce, K.J.R. Rasmussen, Distortional buckling of cold-formed stainless steel sections: finite-element modeling and design, J. Struct. Eng., ASCE 132 (4) (2006) 505–514.
[53] M. Chen, S. Fan, Y. Tao, S. Li, M. Liu, Design of the distortional buckling capacity of stainless steel lipped C-section columns, J. Constr. Steel Res. 147 (2018) 116–131.
[54] N.G. Saliba, L. Gardner, Deformation-based design of stainless steel cross-sections in shear, Thin-Walled Struct. 123 (2018) 324–332.
[55] CECS-410, Technical Specification for Stainless Steel Structures, China Planning Press, Beijing, 2015 (in Chinese).
[56] ASCE, Specification for the Design of Cold-Formed Stainless Steel Structural Members", SEI/ASCE 8-02, American Society of Civil Engineers, New York, 2002 (Standard No. 02-008).
[57] AS/NZS 4673, Cold-formed Stainless Steel Structures, Standards Australia, Sydney, 2001.
[58] K.J.R. Rasmussen, J. Rondal, Strength curves for metal columns, J. Struct. Eng., ASCE 123 (6) (1997) 721–728.
[59] J. Becque, M. Lecce, K.J.R. Rasmussen, The direct strength method for stainless steel compression members, J. Constr. Steel Res. 64 (11) (2008) 1231–1238.
[60] Y. Huang, B. Young, Design of cold-formed stainless steel circular hollow section columns using direct strength method, Eng. Struct. 163 (2018) 177–183.
[61] Arrayago I., Real E., Mirambell E. and Gardner L., "The continuous strength method for stainless steel columns". Proceedings of the Fifth International Experts Seminar on Stainless Steel in Structures, 18th-19th September 2017, London, UK.
[62] S. Ahmed, M. Ashraf, Numerical investigation on buckling resistance of stainless steel hollow members, J. Constr. Steel Res. 136 (2017) 193–203.
[63] M. Anwar-Us-Saadat, M. Ashraf, The continuous strength method for lateral-torsional buckling of stainless steel I-beams, Thin-Walled Struct. 130 (2018) 148–160.
[64] Y. Huang, B. Young, Tests of pin-ended cold-formed lean duplex stainless steel columns, J. Constr. Steel Res. 82 (2013) 203–215.
[65] M. Theofanous, L. Gardner, Testing and numerical modelling of lean duplex stainless steel hollow section columns, Eng. Struct. 31 (12) (2009) 3047–3058.

[66] M. Theofanous, T.M. Chan, L. Gardner, Structural response of stainless steel oval hollow section compression members, Eng. Struct. 31 (4) (2009) 922–934.
[67] B. Young, W.M. Lui, Tests of cold-formed high strength stainless steel compression members, Thin-Walled Struct. 44 (2) (2006) 224–234.
[68] L. Yang, M. Zhao, T.M. Chan, F. Shang, D. Xu, Flexural buckling of welded austenitic and duplex stainless steel I-section columns, J. Constr. Steel Res. 122 (2016) 339–353.
[69] H.X. Yuan, Y.Q. Wang, L. Gardner, Y.J. Shi, "Local–overall interactive buckling of welded stainless steel box section compression members", Eng. Struct. 67 (2014) 62–76.
[70] A.A. de Menezes, P.C.G. da S. Vellasco, L.R.O. de Lima, A.T. da Silva, Experimental and numerical investigation of austenitic stainless steel hot-rolled angles under compression, J. Constr. Steel Res. 152 (2019) 42–56.
[71] M.F. Hassanein, N. Silvestre, Flexural behavior of lean duplex stainless steel girders with slender unstiffened webs, J. Constr. Steel Res. 85 (2013) 12–23.
[72] C. Fang, F. Zhou, C. Luo, Cold-formed stainless steel RHSs/SHSs under combined compression and cyclic bending, J. Constr. Steel Res. 141 (2018) 9–22.
[73] W.M. Lui, M. Ashraf, B. Young, "Tests of cold-formed duplex stainless steel SHS beam–columns", Eng. Struct. 74 (2014) 111–121.
[74] O. Zhao, L. Gardner, B. Young, Buckling of ferritic stainless steel members under combined axial compression and bending, J. Constr. Steel Res. 117 (2016) 35–48.
[75] I. Arrayago, E. Real, E. Mirambell, Experimental study on ferritic stainless steel RHS and SHS beam-columns, Thin-Walled Struct. 100 (2016) 93–104.
[76] I. Arrayago, F. Picci, E. Mirambell, E. Real, Interaction of bending and axial load for ferritic stainless steel RHS columns, Thin-Walled Struct. 91 (2015) 96–107.
[77] O. Zhao, L. Gardner, B. Young, "Testing and numerical modelling of austenitic stainless steel CHS beam–columns", Eng. Struct. 111 (2016) 263–274.
[78] F. Walport, L. Gardner, E. Real, I. Arrayago, D.A. Nethercot, Effects of material nonlinearity on the global analysis and stability of stainless steel frames, J. Constr. Steel Res. 152 (2019) 173–182.
[79] EN 1993-1-1: 2005 +A1:2014. Eurocode 3: Design of Steel Structures. Part 1-1: General Rules and Rules for Buildings, CEN, Brussels, Belgium, 2014.
[80] Walport, F., Gardner, L. and Nethercot, D. A., "A method for the treatment of second order effects in plastically-designed steel frames", Eng. Struct.. Submitted.
[81] K.J.R. Rasmussen, H. Zhang, "Future challenges and developments in the design of steel structures – an Australian perspective", Proceedings of Eurosteel 2018, Copenhagen, Denmark, vol. 1, 2018, pp. 81–94.
[82] S. Shayan, K.J.R. Rasmussen, H. Zhang, On the modelling of initial geometric imperfections of steel frames in advanced analysis, J. Constr. Steel Res. 98 (2014) 167–177.
[83] J.X. Gu, S.L. Chan, Second-order analysis and design of steel structures allowing for member and frame imperfections, Int. J. Numer. Methods Eng. 62 (5) (2005) 601–615.
[84] J.Y.R. Liew, W.F. Chen, H. Chen, Advanced inelastic analysis of frame structures, J. Constr. Steel Res. 55 (2000) 245–265.
[85] M. Kucukler, L. Gardner, L. Macorini, Development and assessment of a practical stiffness reduction method for the in-plane design of steel frames, J. Constr. Steel Res. 126 (2016) 187–200.
[86] W. Liu, K.J.R. Rasmussen, H. Zhang, Systems reliability for 3D steel frames subject to gravity loads, Structures 8 (2016) 170–182.
[87] N.S. Trahair, S.L. Chan, Out-of-plane advanced analysis of steel structures, Eng. Struct. 25 (13) (2003) 1627–1637.
[88] D.W. White, Plastic-hinge methods for advanced analysis of steel frames, J. Constr. Steel Res. 24 (2) (1993) 121–152.
[89] R.D. Ziemian, W. McGuire, G.G. Dierlein, Inelastic limit states design. Part I: planar frame studies, J. Struct. Eng., ASCE 118 (9) (1992) 2532–2549.
[90] L. Gardner, X. Yun, A. Fieber, L. Macorini, Steel design by advanced analysis: material modeling and strain limits, Engineering 5 (2019) 243–249.
[91] C. Buchanan, V.P. Matilainen, A. Salminen, L. Gardner, Structural performance of additive manufactured metallic material and cross-sections, J. Constr. Steel Res. 136 (2017) 35–48.
[92] C. Buchanan, L. Gardner, Metal 3D printing in construction: a review of methods, research, applications, opportunities and challenges, Eng. Struct. 180 (2019) 332–348.
[93] C. Buchanan, W. Wan, L. Gardner, Testing of wire and arc additively manufactured stainless steel material and cross-sections, Ninth International Conference on Advances in Steel Structures (ICASS2018), December 2018, pp. 5–7 Hong Kong, China.